JOURNAL OF GEOPHYSICAL RESEARCH, VOL. 105, NO. B9, PAGES 21,483–21,495, SEPTEMBER 10, 2000

Ground deformation associated with the March 1996 earthquake swarm at Akutan volcano, Alaska, revealed by satellite radar interferometry

Zhong Lu,[1] Charles Wicks Jr.,[2] John A. Power,[3] and Daniel Dzurisin[4]

Abstract. In March 1996 an intense swarm of volcano-tectonic earthquakes (~3000 felt by local residents, M_{max} = 5.1, cumulative moment of 2.7 x 10^{18} N m) beneath Akutan Island in the Aleutian volcanic arc, Alaska, produced extensive ground cracks but no eruption of Akutan volcano. Synthetic aperture radar interferograms that span the time of the swarm reveal complex island-wide deformation: the western part of the island including Akutan volcano moved upward, while the eastern part moved downward. The axis of the deformation approximately aligns with new ground cracks on the western part of the island and with Holocene normal faults that were reactivated during the swarm on the eastern part of the island. The axis is also roughly parallel to the direction of greatest compressional stress in the region. No ground movements greater than 2.83 cm were observed outside the volcano's summit caldera for periods of 4 years before or 2 years after the swarm. We modeled the deformation primarily as the emplacement of a shallow, east-west trending, north dipping dike plus inflation of a deep, Mogi-type magma body beneath the volcano. The pattern of subsidence on the eastern part of the island is poorly constrained. It might have been produced by extensional tectonic strain that both reactivated preexisting faults on the eastern part of the island and facilitated magma movement beneath the western part. Alternatively, magma intrusion beneath the volcano might have been the cause of extension and subsidence in the eastern part of the island. We attribute localized subsidence in an area of active fumaroles within the Akutan caldera, by as much as 10 cm during 1992-1993 and 1996-1998, to fluid withdrawal or depressurization of the shallow hydrothermal system.

1. Introduction

Akutan volcano, situated in the west central part of Akutan Island in the eastern part of the Aleutian volcanic arc, is a composite stratovolcano with a circular summit caldera ~2 km across and 60-365 m deep. An active cinder cone located in the northeast quarter of the caldera is ~1 km wide and 240 m high [*Newhall and Dzurisin*, 1988; *Miller et al.*, 1998] (Figure 1). Three small, sulfur-lined craters occupy its summit, and several fumarolic areas are present along its south and southwest flank. The Akutan caldera rim reaches a maximum altitude of 1303 m at Akutan Peak. A breach in the caldera rim to the north channels volcanic flows from intracaldera vents in that direction. The island is sparsely inhabited, with a seasonal population of about 750 people in the city of Akutan, 13 km east of the volcano's summit. The larger communities of Unalaska and Dutch Harbor lie 50 km to the southwest on Unalaska Island, which includes Makushin volcano. The eastern part of Akutan Island consists mainly of deposits from an ancestral Akutan volcano and older, undifferentiated volcanic rocks ranging in age from 1.5 to 3.3 Ma [*Richter et al.*, 1998].

Akutan is one of the most active volcanoes in the Aleutian volcanic arc. At least 27 separate eruptive episodes have been noted since 1790, and additional events have probably gone unrecorded [*Miller et al.*, 1998]. Most of the reported eruptions included small-to-moderate explosions (volcanic explosivity index (VEI) 2) from the active intracaldera cone. In 1929, lava flowed out of the caldera rim gap ~0.7 km down the northeast flank, triggering small lahars that flowed into valleys to the north and northwest [*Finch*, 1935]. An explosive eruption in 1948 produced measurable amounts of ash in the city of Akutan. This eruption was preceded by three earthquakes that were felt strongly in Akutan Village [*Alaska Sportsman*, 1949]. In 1978, airline pilots observed large incandescent bombs ejected more than 100 m above the summit, and lava again flowed down the volcano's north flank. The most recent eruptive activity was a series of small (VEI 1) steam and ash emissions during March-May 1992. Little is known about Akutan's seismic activity prior to 1996 or about the composition of its eruptive products, except that most are tholeiitic basalts or andesites, with 50.3-62.9% SiO_2 [*Miller et al.*, 1998; *Richter et al.*, 1998].

1.1. March 1996 Earthquake Swarm

Beginning early on March 11, 1996, Akutan Island was struck by an intense swarm of earthquakes that lasted ~11 hours. The swarm consisted of more than 80 earthquakes with

[1]Raytheon STX Corporation, U.S. Geological Survey, EROS Data Center, Sioux Falls, South Dakota.
[2]U.S. Geological Survey, Menlo Park, California.
[3]U.S. Geological Survey, Alaska Volcano Observatory, Anchorage.
[4]U.S. Geological Survey, David A. Johnston Cascades Volcano Observatory, Vancouver, Washington.

Paper number 2000JB900200.
0148-0227/00/2000JB900200$09.00

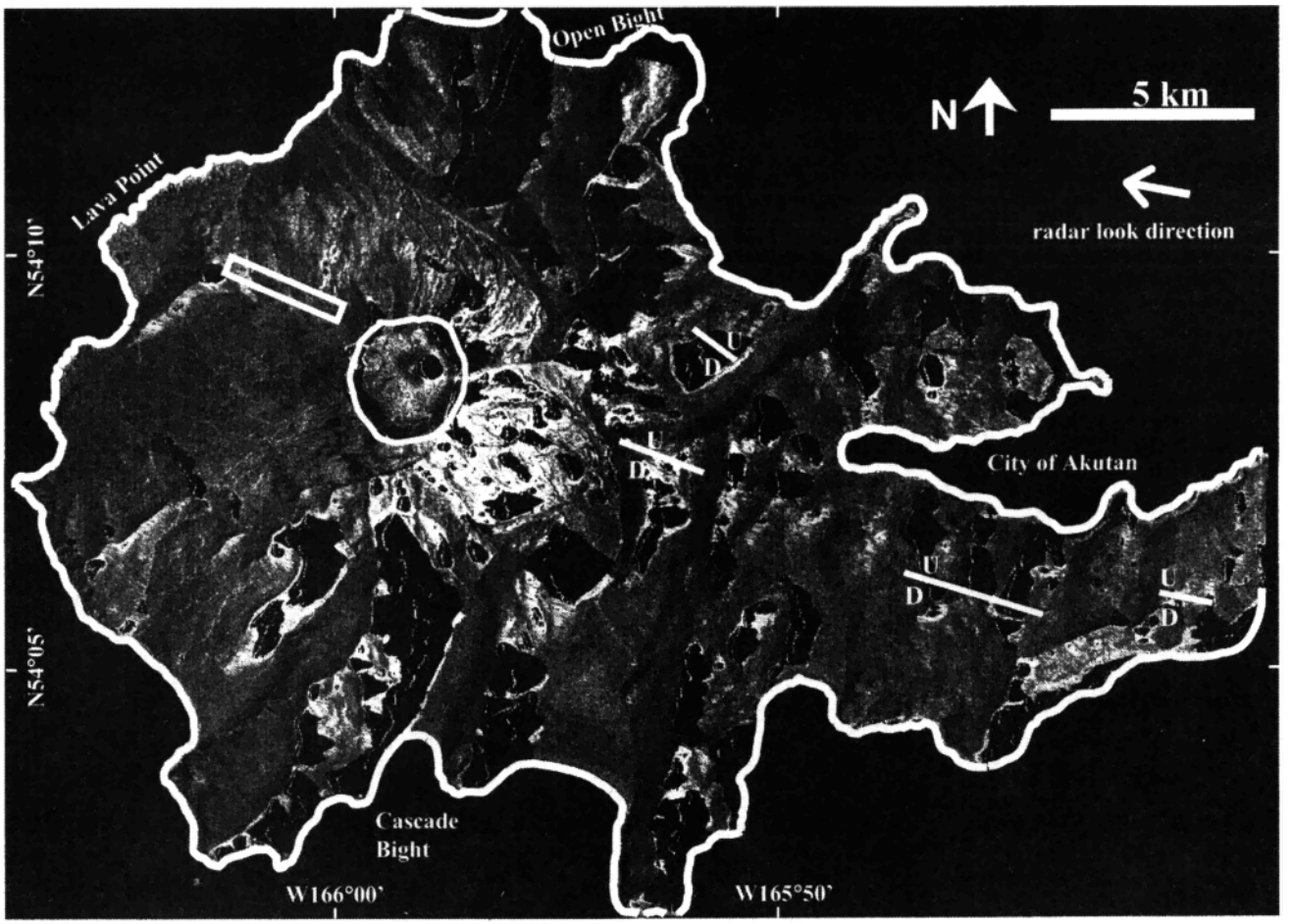

Figure 1. ERS-1 SAR amplitude image of Akutan Island. Dark regions indicate areas with severe geometric distortion in the SAR images. Coastline and caldera rim are drawn in white. The white rectangle on the northwest of the island represents a zone of ground cracks that formed during the March 1996 earthquake swarm. Normal faults reactivated on the east of the island during the March 1996 earthquake swarm are drawn in white lines, and U and D represent the upthrown and downthrown sides of the faults.

magnitude >3.5 (M_{max} = 5.1). A second, more vigorous swarm on March 14 lasted ~19 hours and included more than 120 earthquakes with magnitude >3.5. Thousands of smaller earthquakes also occurred during these periods of strong activity. Hereinafter we refer to the entire earthquake sequence as the March 1996 swarm. The estimated total cumulative seismic moment of the swarm is 2.7 x 10^{18} N m (Figure 2) [*Power et al.*, 1996], roughly equivalent to a single magnitude 6.0 earthquake. Seismic energy released at Akutan volcano between March 11 and 14 is comparable to that released between March 20 and May 24, 1980, before the eruption of Mount St. Helens [*Endo et al.*, 1981]. The Akutan seismic energy is considerably higher than those from precursory seismic sequences before recent eruptions at Mount Spurr and Redoubt volcanoes in the central Aleutians [*Power et al.*, 1994, 1995]. It is also higher than that from the 1988 seismic swarm at Mount Dutton volcano, Alaska, which did not result in an eruption. During the height of activity, residents of Akutan Island reported feeling continuous low-level ground shaking punctuated by individual shocks about once per minute. The shaking caused considerable discomfort among the residents, many of whom voluntarily left the island. Residents continued to feel occasional earthquakes for several months after the swarm's peak in March 1996. The Alaska Volcano Observatory (AVO) first deployed a single seismometer in the city of Akutan on March 12 and then a network of four telemetered stations on the eastern side of the island by March 18. An island-wide network of six permanent stations was installed during July 1996.

In July 1996, AVO scientists discovered fresh ground cracks that extended discontinuously from near Lava Point to the southeast side of Akutan Island (strike ~N70°W; Figure 1). The orientation of the observed ground cracks fits well with the regional tectonic stress regime [*Nakamura et al.*, 1977; *Nakamura and Uyeda*, 1980] and is approximately parallel to the direction of relative motion between the Pacific and North American Plates (see Section 4). The cracks broke snowfields, and their sides showed little evidence of erosion, suggesting they had formed recently, almost surely during the March 1996 swarm. The most extensive cracks occurred in a zone roughly 500 m wide and 3 km long between Lava Point and the summit of Akutan volcano. Local graben structures with vertical displacements of 30-80 cm suggest that the cracks formed in response to tumescence of the volcano's northwest flank. The cracks on the east side of the island are only a few centimeters wide and apparently represent activation of Holocene normal faults [*Richter et al.*, 1998].

More than 1300 earthquakes were located at Akutan Island between March 18 and July 26, 1996. The majority of these earthquakes form a prominent cluster near the head of Akutan

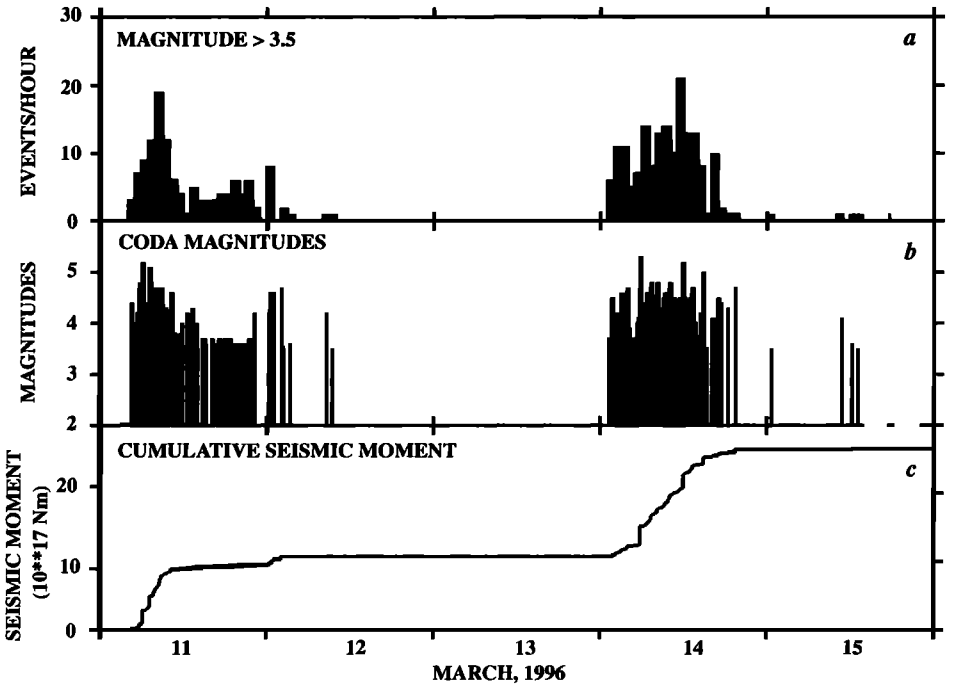

Figure 2. Time series showing (a) the number of earthquakes per hour with magnitude >3.5, (b) coda magnitudes, and (c) cumulative seismic moment for Akutan earthquakes during March 11-15, 1996. Data are from recordings at station DTN on the flank of Dutton volcano, 250 km east of Akutan.

Harbor (Figure 3). Seismic activity in this area was quite high when the temporary stations were first deployed in March 1996 and declined rapidly almost to quiescence by the time the permanent network became operational in late July 1996. Well-located earthquakes in this cluster range in depth from roughly sea level to ~8 km. To test the reliability of these depths, we located a suite of ~400 events from this cluster that each contained at least four *P* arrivals and two *S* arrivals, using several velocity models. There was little change in the depth distribution, suggesting that the depth determinations are relatively robust. Earthquakes within this cluster dip steeply to the northeast, but the dip angle is strongly dependent on the velocity model and therefore the dip is poorly constrained. Owing to the network geometry, earthquakes that might have occurred under Lava Point or the Akutan caldera in the northwest part of the island would have been mostly overlooked, unless they were large enough to be detected by the four stations in the eastern part of the island. Locations of some of the earthquakes in the cluster beneath the eastern part of the island might have been biased for the same reason, i.e., the limited number of temporary stations and the network geometry.

Between March 18 and July 26, 1996, we also observed a small number of epicenters that extend southeastward from the strong cluster near the head of Akutan Harbor to the tip of the island. The depths of well-located earthquakes in this group range from 2 to 6 km (Figure 3a). Although the accuracy of these locations is poor, on the basis of the order of arrival times at the temporary stations we are convinced that the epicenters extend across the southeast part of the island. Our confidence is bolstered by additional earthquakes that were located in this area after the permanent network was installed (Figure 3b).

As soon as the permanent network became operational on July 26, we began to locate earthquakes beneath the Akutan caldera and Lava Point, as well as in the previously recognized active areas near the head of Akutan Harbor and the southeast part of the island (Figure 3b). The earthquakes beneath Lava Point are located mainly between depths of 5 and 9 km, while those beneath the caldera cluster are located between 1 and 4 km depth. Taken in total, the earthquake epicenters form a diffuse NW–SE band that extends from Lava Point to the southeast shore of the island (Figure 3b) and approximately aligns with the fresh ground cracks on the western and eastern parts of the island. From August 1, 1996, to December 31, 1998, we located more earthquakes under Lava Point and the Akutan caldera than near the city of Akutan, which suggests that a similar pattern might have held from March 18 to July 26, 1996. We suspect that areas beneath the caldera and Lava Point were seismically active throughout 1996, but the temporary network lacked sufficient coverage to detect or locate earthquakes there between March and July. Therefore we mainly used the seismicity pattern from August 1, 1996, to December 31, 1998 to constrain deformation models (see Section 3).

1.2. Synthetic Aperture Radar Interferometry Studies of Aleutian Volcanoes

Repeat-pass synthetic aperture radar (SAR) interferometry has become an important technique to measure volcanic deformation at a horizontal resolution of tens of meters with a vertical accuracy of centimeters to subcentimeters. Deformation measured with repeat-pass SAR interferometry has been reported for numerous volcanoes worldwide [e.g., *Massonnet et al.*, 1995; *Rosen et al.*, 1996; *Lu et al.*, 1997, 1998, 2000a, 2000b; *Sigmundsson* et al., 1997, 1999; *Thatcher and Massonnet*, 1997; *Fujiwara et al.*, 1998; *Lanari et al.*, 1998; *Wicks et al.*, 1998; *Jonsson et al.*, 1999].

SAR interferometry has recently been applied to study ground deformation at several Aleutian volcanoes [*Lu et al.*,

1997, 1998, 2000a, 2000b]. The first application was at New Trident volcano, located ~800 km northeast of Akutan. An ERS-1 interferogram indicated ~7-9 cm of uplift from 1993 to 1995 [*Lu et al.*, 1997]. Numerical modeling suggested inflation of a magma body located ~2 km beneath the volcano. Shortly thereafter, AVO geologists noted signs of dome-like uplift and fumarolic activity at New Trident (J. Eichelberg, personal communication, 1997).

An intensive SAR interferometric study was made of the February-April 1997 eruption of Okmok volcano, ~170 km southwest of Akutan. Interferograms constructed from C-band ERS-1/ERS-2 SAR images indicated (1) ~18 cm of uplift between 1992 and 1995, (2) more than 140 cm of subsidence associated with the 1997 eruption, and (3) ~10 cm of uplift in the first year after the eruption [*Lu et al.*, 1998, 2000a]. Numerical modeling suggests that the magma reservoir responsible for the eruption was located ~2.7 km beneath the center of the caldera, ~5 km from the eruptive vent. The lower bound for the volume of material erupted is 0.055 km^3, and the estimated average thickness of the 1997 lava flow is 7.4 m [*Lu et al.*, 1998, 2000a].

SAR interferometry has also been applied at Westdahl volcano, ~100 km northeast of Akutan. ERS-1/ERS-2 interferograms mapped progressive uplift of the volcano at a rate of ~3 cm/yr during a 6-year period of quiescence following its most recent eruption in 1991-1992 [*Lu et al.*, 2000b]. This study demonstrated that SAR interferometry is a useful tool to prospect for magma bodies by detecting deformation that is virtually aseismic and therefore difficult to detect by conventional means.

Reduction of radar coherence is the major obstacle to applying SAR interferometry on Aleutian volcanoes. Radar returns must be coherent in order for useful information to be derived from interferograms. This is a fundamental assumption during the generation of an interferogram from a pair of SAR images acquired at different times. At Aleutian volcanoes, processes that reduce interferometric coherence include snow/ice melting and accumulation, freezing/thawing of surface material, and erosion/deposition of volcanic ash. Therefore the best chance of producing coherent interferograms comes from using images that were acquired during summer or early fall, separated in time by 1 year to a few *years [Lu and Freymueller*, 1998].

In this study, we produce several interferograms for Akutan Island from 1992 to 1998 and explore various numerical models to help constrain the processes responsible for the March 1996 earthquake swarm. This is the first geodetic measurement conducted for this volcano. We conclude that the swarm was caused at least in part by inflation of a magma body beneath Akutan volcano and

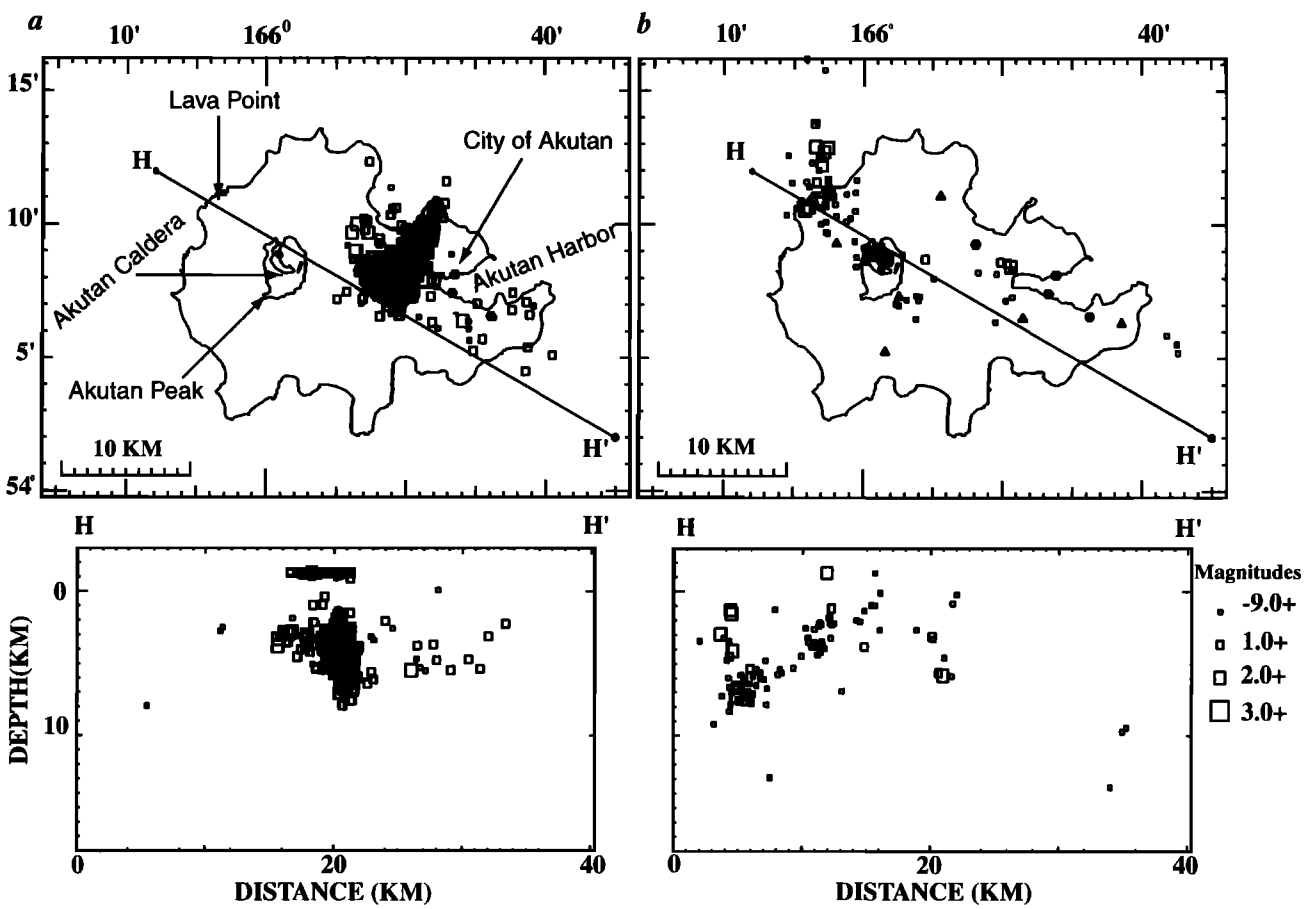

Figure 3. (a) Epicenter map and cross section (H-H′) of earthquakes located at Akutan Island between March 18, 1996, and July 26, 1996. Hypocenters were calculated using only the four temporary stations (hexagons) located on the eastern side of the island. (b) Same as Figure 3a, except for the period from August 1, 1996, to December 31, 1998. Hypocenters were calculated using all available data from both temporary (hexagon) and permanent (triangle) stations on Akutan Island. Earthquake magnitude scale applies to both plots.

Table 1. Interferometric Data Acquisition Parameters

Orbit 1	Orbit 2	Date 1	Date 2	h_a[a], m	Plate
E1_10967	E2_7670	Aug. 20, 1993	Oct. 7, 1996	1818	1a
E1_20329	E2_11177	June 4, 1995	June 9, 1997	157	1b
E1_6186	E1_11196	Sept. 20, 1992	Sept. 5, 1993	166	2a
E1_11969	E1_2660	Oct. 29, 1993	Oct. 23, 1995	60	
E2_7670	E2_13181	Oct. 7, 1996	Oct. 27, 1997	100	
E2_11177	E2_17690	June 9, 1997	Sept. 7, 1998	84	
E2_6668	E2_17690	July 29, 1996	Sept. 7, 1998	55	2b

[a]Altitude of ambiguity is h_a.

intrusion of a dike to within a few hundred meters of the surface.

2. Radar Observations of Ground Deformation

To study ground deformation associated with the March 1996 swarm, we used two-pass SAR interferometry with images acquired by the European Space Agency (ESA) ERS-1 and ERS-2 satellites. For a discussion of the technique, see *Rosen et al.* [1996] and *Massonnet and Feigl* [1998]. Because interferometric coherence for C-band (wavelength of 5.66 cm) radar images persists for up to several years at Aleutian volcanoes where the surface is snow-free and dominated by lava [*Lu and Freymueller*, 1998], we constructed interferograms using images acquired each summer or early fall from 1992 to 1998, except in 1994 (Table 1).

Topographic effects were removed using the U.S. Geological Survey (USGS) 15-min Alaska digital elevation model (DEM), with 2 arc sec latitude posting (~60 m) and 3 arc sec longitude posting (~60 m). The specified horizontal accuracy of the DEM is ~60 m, and the root-mean-square vertical error is ~15 m [*Gesch*, 1994]. In two-pass SAR interferometry, errors in the DEM are mapped into apparent deformation of the ground surface. This effect is characterized by a term called the altitude of ambiguity, h_a, which is the amount of topographic error required to generate one interferometric fringe in a topography-removed interferogram [*Massonnet and Rabaute*, 1993]. For example, a 100-m DEM error would produce one spurious fringe in an interferogram with h_a = 100 m or two spurious fringes in an interferogram with h_a = 50 m. To minimize the effect of possible DEM errors, we chose image pairs with the largest available altitudes of ambiguity (60 to 1818 m).

Plate 1a shows a deformation interferogram for the period from August 20, 1993, to October 7, 1996, which brackets the March 1996 earthquake swarm. The altitude of ambiguity of the image pair is 1818 m, so the interferogram is insensitive to any plausible errors in the DEM. There are more than 21 fringes from A to B on the northwestern flank of Akutan volcano. Each fringe represents 2.83 cm (half the radar wavelength) of range change along the satellite look direction. The right-looking ERS satellites orbit over Akutan volcano from north to south with a track angle of S16°W. The look direction of the satellites is ~23° from vertical, so interferograms formed from ERS images are sensitive mostly to vertical ground movements. In this case, the pattern of color changes from A to B indicates that A moved toward the satellite vantage point (i.e., upward) by ~60 cm with respect to B. Similarly, there are more than 8 fringes from C to D, which indicates that C moved upward ~23 cm relative to D. Interferometric coherence was maintained reasonably well over this 3-year period in areas covered by lava flows. Areas where coherence was lost correspond mostly to alluvium.

We verified this result by forming an independent interferogram with images acquired on June 4, 1995, and June 9, 1997 (Plate 1b). The h_a of this image pair is ~160 m, so the interferogram is more sensitive to any errors in the DEM. However, no such topographic artifacts are apparent in the interferogram, which shows essentially the same deformation pattern as Plate 1a. Even though the interferograms in Plate 1 span ~3 years and ~2 years, respectively, the interferometric coherence is generally higher in Plate 1a. This might be due to the fact that the images used in Plate 1b were acquired in June, before seasonal snow and ice had completely melted. The larger h_a for the interferogram in Plate 1a probably also contributed to its greater coherence because it means that the baseline separation for the images represented in Plate 1a was smaller than for Plate 1b (i.e., the images were acquired from closer vantage points in the first case).

The fact that two interferograms formed from independent image pairs with very different altitudes of ambiguity show essentially the same deformation pattern means that the pattern is not an artifact of orbital errors, topographic errors, or atmospheric disturbances. Instead, the fringes map out ground deformation that must have occurred during the time period of overlap in the interferograms, between June 1995 and October 1996, almost surely during the March 1996 earthquake swarm.

Several features common to both interferograms in Plate 1 are worth summarizing. These observations provide important constraints on source models used to simulate the observed deformation.

1. The patterns of color changes, which indicate the progressively increasing or decreasing phase of ground-reflected radar waves (i.e., movement of the ground surface away from or toward the satellite position, respectively), are opposite for the western and eastern parts of the volcano. Whereas the western part of the island including Akutan volcano moved upward, most of the eastern part moved downward. The center axis of the uplift aligns with the zone of fresh ground cracks observed on the northwest flank of the volcano. The axis of the subsidence is roughly parallel to the

orientation of several Holocene normal faults mapped by *Richter et al.* [1998], several sections of which were rejuvenated during the March 1996 earthquake swarm. Line EF, from near Open Bight on the north coast to near Cascade Bight on the south coast, approximately divides the uplifted western part of the island from the down-warped eastern part.

2. The pattern of fringes west of Open Bight, where progressively more uplift was observed toward the summit of the volcano, is dramatically different from that east of Open Bight, where gentle subsidence occurred.

3. Fringes are asymmetric on the western flanks of the volcano. They are denser (i.e., more concentrated deformation) to the north of the ground cracks than to the south. Near Lava Point, fringes gradually bend into the ocean.

4. Several fringes were observed north of city of Akutan, indicating downward movement toward the center of the island.

5. Fringes in several areas with high interferometric coherence on the eastern part of the island, outlined by the white dashed polygons in Plate 1a, indicate subsidence along an axis approximately parallel to the normal faults. Although these areas are not extensive enough to reveal the mode of deformation entirely, they suggest broad downwarping along the W-E center axis of the island rather than faulting along the normal faults mapped by *Richter et al.* [1998], most of which step down to the south.

We also looked for evidence of ground deformation at Akutan for several years before and after the March 1996 swarm by producing four interferograms spanning the following time intervals (Table 1): (1) September 1992 to September 1993 (h_a = 166 m), (2) October 1993 to October 1995 (h_a = 60 m), (3) October 1996 to October 1997 (h_a = 100 m), and (4) June 1997 to September 1998 (h_a = 84 m). Coherence was generally good outside the caldera, where we observed no deformation greater than one fringe in any of the interferograms. Inside the caldera, coherence was generally poor as a result of persistent snow cover. However, two of the interferograms from images acquired between the end of July and the end of September were coherent enough to reveal deformation associated with a zone of active fumaroles in the south and southwest part of the caldera.

Plate 2a shows a portion of an interferogram spanning September 20, 1992, to September 5, 1993 (h_a = 166 m). The fringe pattern inside the caldera indicates that point B subsided ~3 cm with respect to the point A, as shown in the profile in Figure 4. A similar pattern occurs in an interferogram spanning July 29, 1996, to September 7, 1998 (h_a = 55 m). In this case, point B subsided ~10 cm with respect to point A (Plate 2b and Figure 4). The height difference between A and B is <180 m, so the apparent deformation is unlikely to be a spurious topographic effect. It is also unlikely that the fringes are caused by atmospheric delay anomalies [*Delacourt et al.*, 1998; *Lu et al.*, 2000a; *Zebker et al.*, 1997], because (1) we observed the deformation in two independent interferograms, (2) such anomalies typically occur over length scales of several kilometers, (3) atmospheric delay anomalies are generally less than one to two fringes for Okmok volcano, 170 km west of Akutan [*Lu et al.*, 200a], and (4) tropospheric anomalies are negligible because the height difference from A to B is <80 m. Snow cover that usually persists in the caldera for more than 10 months of the year makes it difficult to study deformation there with ERS interferometry because only a small number of images can be acquired under snow-free conditions each year.

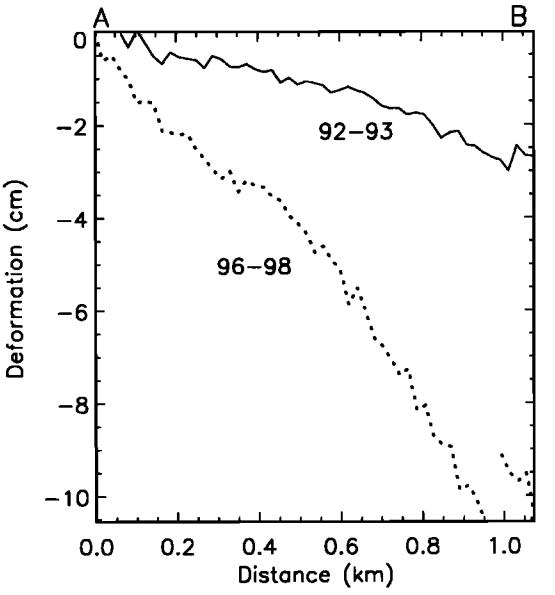

Figure 4. Deformation profiles show progressive subsidence from A to B (Plate 2) during the two time intervals. The subsidence patterns and average subsidence rates are similar.

3. Deformation Modeling

The complexity of the deformation pattern revealed by the interferograms in Plate 1 and the patch-like nature of coherent areas make it difficult to identify a unique model for the deformation sources. The earthquake distribution from March 18 to July 26, 1996, is a poor guide to the geometry and location of sources for reasons discussed earlier. However, with the geometry of new surface fractures and the pattern of seismicity from August 1996 to December 1998 as constraints, we explored several models using a conventional buried point source [*Mogi*, 1958] and elastic dislocations [*Okada*, 1985]. Our preferred model successfully explains most of the observations. The main assumption used in constructing the models is that the crust beneath Akutan Island is an isotropic, elastic half-space. The pattern of range changes produced by dislocation sources was calculated using computer programs written by *Feigl and Dupre* [1999].

The interferogram shown in Plate 1a was "unwrapped" using the technique described by *Goldstein et al.* [1988]. In areas with good coherence and clearly differentiated fringes, repetitive phase values ranging from 0 to 2π can be unwrapped to produce a cumulative displacement field. Owing to the patch-like nature of the coherent areas (Plate 1a), we developed a technique to unwrap the 12 regions with good coherence separately and then mosaic the pieces together (Plate 3a). We carefully examined the unwrapped interferogram to ensure that no artifacts were created during the unwrapping process.

The Mogi source consists of four model parameters: the (x, y) location coordinates, depth, and volume change. The rectangular elastic dislocation source consists of 10 model parameters: the (x, y) location coordinates; depth, length and

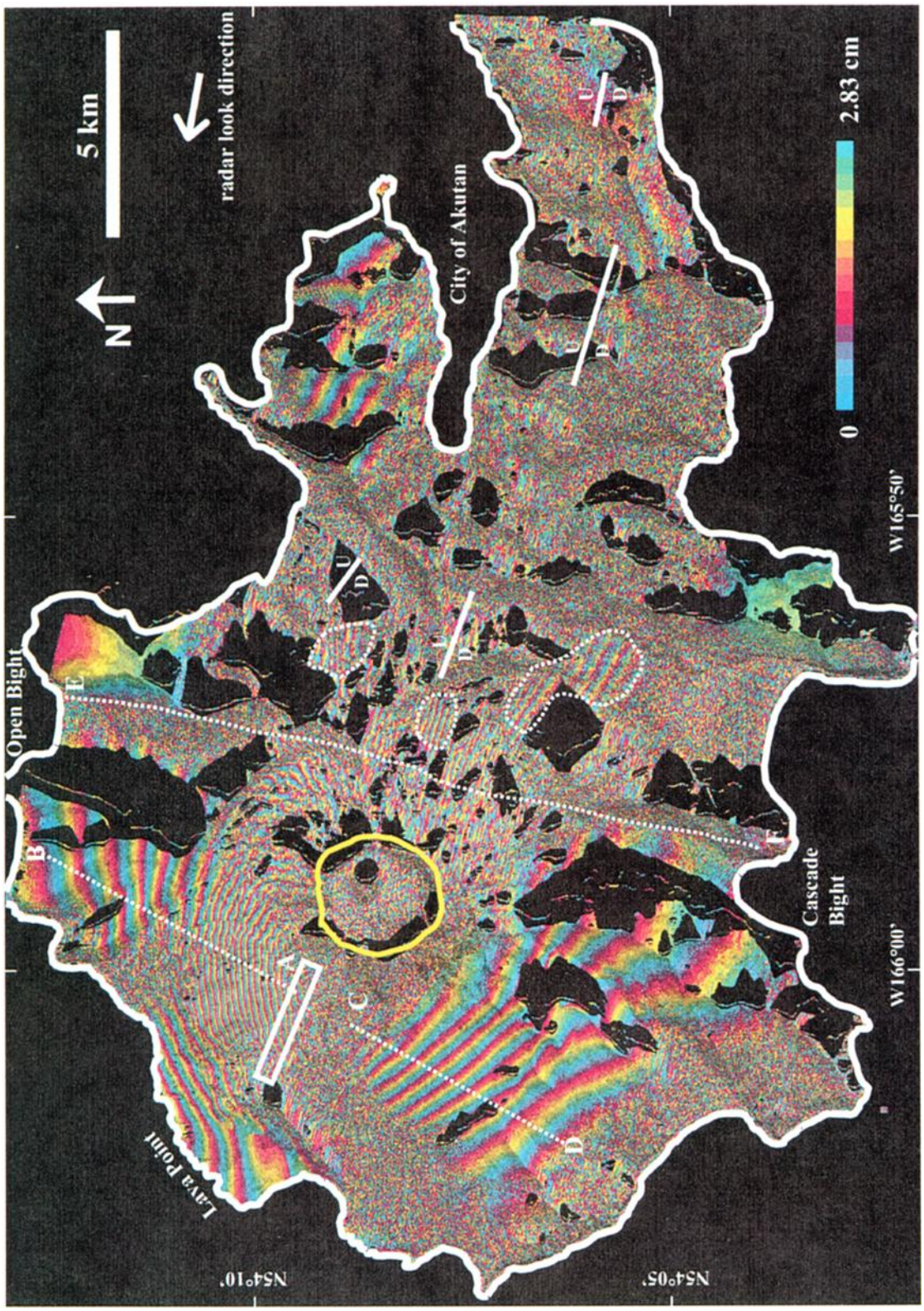

Plate 1a. Deformation interferogram of Akutan Island for the period from August 20, 1993, to October 7, 1996 (h_a = 1818 m). Each fringe (complete color cycle) represents a 2.83 cm range change in the radar look direction. Fringes in several areas with high interferometric coherence on the eastern part of the island are outlined by the white dashed polygons. Line EF approximately divides the uplifted western part of the island from the downwarped eastern part. See Figure 1 for explanation of other features.

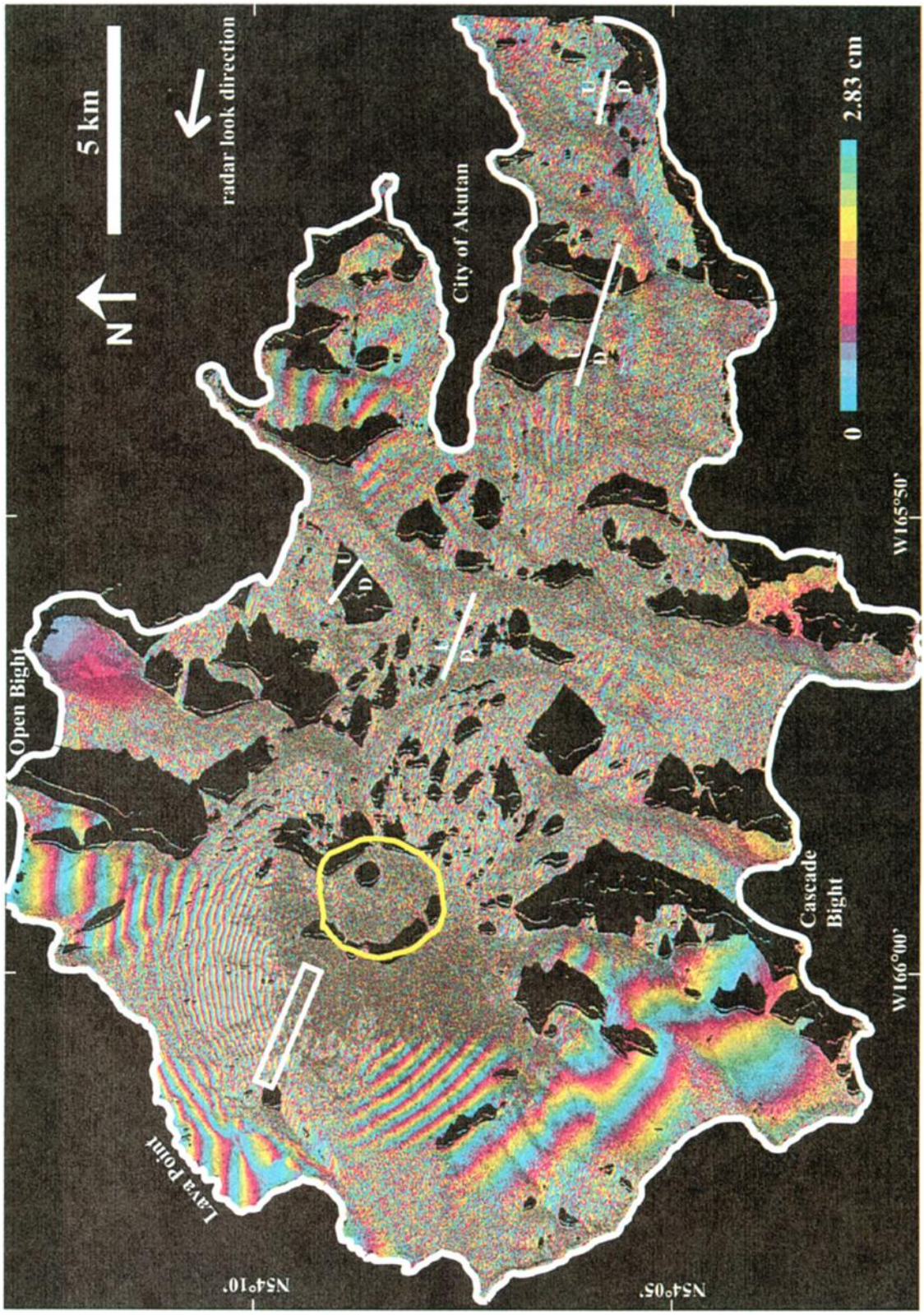

Plate 1b. Interferogram for the period from June 4, 1995, to June 9, 1997. Each fringe (complete color cycle) represents a 2.83 cm range change in the radar look direction. The fringe pattern is essentially the same in the two interferograms (Plates 1a and 1b), which both span the March 1996 swarm and were formed from two independent image pairs. See Figure 1 for explanation of other features.

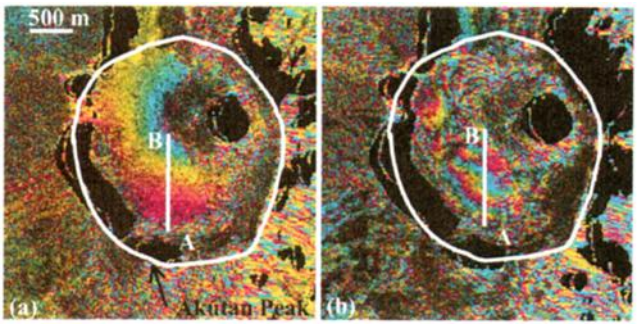

Plate 2. (a) Interferogram in the summit area spanning September 20, 1992, to September 5, 1993 (h_a = 166 m). (b) Interferogram in the summit area spanning July 29, 1996, to September 7, 1998 (h_a = 55 m). The deformation profiles from A to B are shown in Figure 4.

width; three components of slip (two in the plane of the dislocation surface and one perpendicular to it); strike; and dip of the dislocation surface. Because the ground cracks on the northwest flank of the volcano (Figure 1) suggest only expansion (slip directed outward from a dislocation surface), we did not solve for the in-plane components of slip. Therefore the dislocation sources that we modeled consisted of eight parameters. Because the interferogram was unwrapped in a piecewise manner, it yielded 12 separate patches of range change data. We therefore introduced 12 "shift" parameters, which enabled us to solve for a best fit static range change corresponding to each patch. These parameters are necessary because of the unknown amount of range change offset between the "seed points" used to unwrap each patch. We first used forward modeling to identify a reasonable starting model, then modeled the unwrapped interferogram (Plate 3a) by employing the Levenberg-Marquardt method, a nonlinear least squares technique [e.g., *Press et al.*, 1992] that iteratively improves the trial solution until the chi-square difference between the observed and modeled interferogram effectively stops decreasing.

We started with only one Mogi source, then only one dike source, and finally one Mogi source plus one dike. For each iteration of modeling, we calculated a residual image, which is the difference between observed and modeled range change. We chose the following criteria to evaluate the modeling results (Table 2): (1) variance of residual image; (2) variance reduction in percentage, which is defined as $(\sigma_{data} - \sigma_{res})/\sigma_{data}$, where σ_{data} and σ_{res} are variances of observed and residual data; (3) sum-squared errors ($\sum e^2$) of the residual; and (4) signal modeled in percentage, which is defined as $(\sum \Delta_{data}^2 - \sum \Delta_{res}^2)/\sum \Delta_{data}^2$, where Δ_{data} and Δ_{res} are observed and residual range change.

There are about 42,689 pixels in the unwrapped interferogram (Plate 3a), mostly in two patches: one situated on the northwestern part of the island and one on the southwestern part (hereafter called patch 1 and patch 2, respectively). Assuming the deformation field is continuous between patch 1 and patch 2 and because the ground cracks between the caldera and Lava Point (Plate 3a) do not indicate normal faulting, we estimated the differential shift between the patches to be about 0~150 mm. Because 80% of the total deformation values are in patches 1 and 2 the amount of differential shift is an important parameter for modeling.

The results of modeling a single Mogi source delineate two distinct minima: one deep and one shallow (Table 2). Although the improvement in variance and sum-squared errors is only marginally better for a composite source (Mogi plus dislocation) over the single dislocation source (Table 2), the composite source is our preferred model for two reasons. First, the relative shift of range change between patch 1 and patch 2 (shift 1 – shift 2 in Table 2) is more reasonable for the composite source than for the single dislocation source. Second, the fringe gradient on the northwest flank of the volcano is much higher than on the rest of the west end of the island, suggesting at least two sources of deformation. Note that modeling the composite source while forcing the shift between patches 1 and 2 to be zero yields a model with parameters that fall within the 95% confidence limits estimated for the best fit composite model in Table 2.

Of the two sources in the preferred composite source, the dike source is better constrained. We perturbed some of the model parameters one at a time and used an F test to estimate 95% confidence limits of the more important parameters. The 95% confidence interval for the depth to the top of the dike is 0.28 to 0.65 km, whereas the 95% confidence interval for the depth of the Mogi source is 10.6 to 18.0 km. The 95% confidence interval for the volume increase associated with the dike is 0.031 to 0.038 km^3, whereas for the Mogi source it is 0.08 to 0.55 km^3. The 95% confidence ranges for the location of the Mogi source are 6.0 to 10.2 km in N-S direction and 4.9 to 6.8 km in E-W direction. As a side note, we also tried a modeling scheme that simultaneously minimized the relative shift between the two patches. The results indicated that the Mogi source could be as shallow as ~8 km. Some of our earlier modeling efforts aimed at maximizing the global coherence [*Vadon and Sigmundsson*, 1997] resulted in a Mogi source at a depth of 7 km, located almost directly beneath the summit caldera. A more rigorous comparison of the results from different modeling techniques must be assigned to a future study.

Even though the preferred composite source successfully models 99% of the signal in the unwrapped interferogram, it is clear from the residual interferogram in Plate 3e that the deformation field on the east side of the island has not been adequately modeled. We attempted to model the subsidence observed there using various contracting sources. These efforts led to only a modest increase in the overall fit, so they are not discussed further here. The mechanism responsible for subsidence on the east side of the island therefore remains unknown.

We did not attempt to model the source responsible for intracaldera subsidence (Plate 2 and Figure 4), but it is clear from the localized nature of the deformation that the source is shallow, probably within 2 km of the surface. We infer that the source is closely associated with fumarolic areas on the south and southwest flank of the active intracaldera cone. Presumably, subsidence results from fluid loss or depressurization of a shallow hydrothermal system that supplies the fumaroles.

4. Discussion

4.1. SAR Interferometry Compared to Conventional Geodetic Techniques

The complexity of the 1996 deformation field at Akutan makes SAR interferometry very attractive because of its

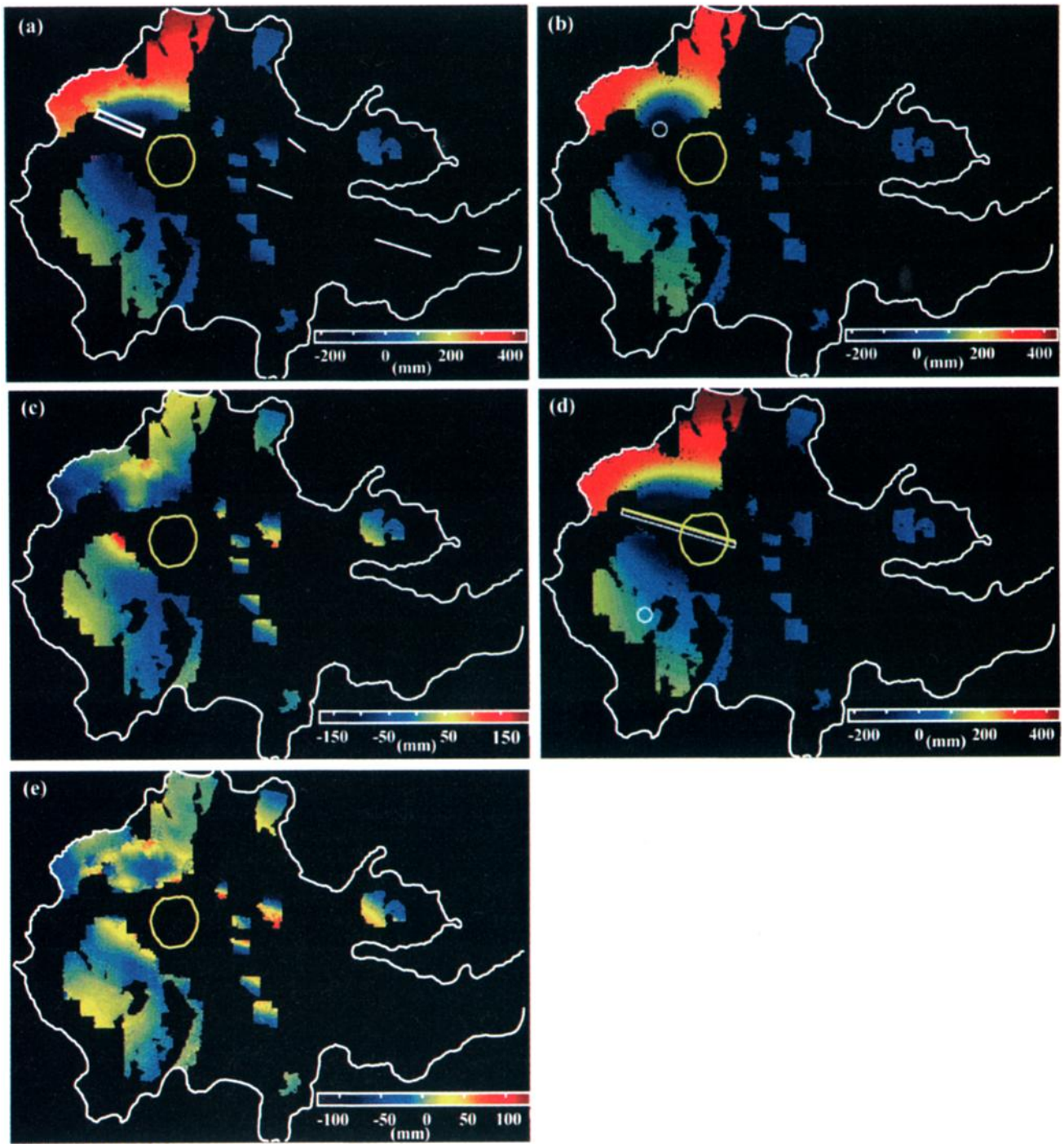

Plate 3. (a) Observed unwrapped interferogram, showing range change at coherent regions. The white rectangle on the northwest of the island represents a zone of ground cracks that formed during the March 1996 earthquake swarm. Normal faults reactivated on the east of the island during the March 1996 earthquake swarm are drawn in white lines. (b) Synthetic interferogram showing range change from the best fitting Mogi source (Table 2). The white circle represents the surface projection of the best fitting source. (c) Residual interferogram showing the difference between the observed (Plate 3a) and synthetic (Plate 3b) interferograms. (d) Synthetic interferogram showing range change from the best fitting Mogi and dislocation sources (Table 2). The white circle and rectangle represent the surface projection of the best fitting sources. Bottom edge of the surface projection of the dislocation is drawn in yellow. (e) Residual interferogram showing the difference between the observed (Plate 3a) and synthetic (Plate 3d) interferograms. Only data points that are successfully unwrapped and used in the modeling are shown. Dark regions indicate areas with severe geometric distortion in the SAR images and/or low interferometric coherence. Coastline is drawn in white, and caldera rim is drawn in yellow.

ability to map surface deformation in two spatial dimensions, even though it measures only the component of surface deformation along the satellite look direction. To adequately characterize such a complex deformation field using a more conventional geodetic technique, such as electronic distance measurement (EDM), tiltmeters or strain meters, or even the Global Positioning System (GPS), would require measurements at a very large number of bench marks. For remote volcanoes, such as those in the Aleutian arc, the resulting workload would be prohibitive. A conventional geodetic network would have to be extensive enough to capture the entire deformation field at each potentially active volcano and also dense enough to adequately characterize possible small-scale complexities. This approach would be subject to numerous pitfalls. For example, if two GPS stations were inadvertently placed along the same interferometric fringe, no relative displacement would be measured even during periods of active deformation. SAR interferometry overcomes this limitation of conventional geodesy, at least in areas of adequate coherence, by providing a more spatially complete image of the deformation field. In the future, combining single-component measurements from SAR interferometry with three-dimensional measurements from GPS will almost surely advance our understanding of the dynamics of magmatic processes.

4.2. Interpretation of the March 1996 Swarm and Future Challenges

The orientation of the observed ground cracks associated with 1996 seismic swarm and the distribution of seismicity from August 1996 to December 1998 fit well with the regional tectonic stress regime. Stress orientations in the Aleutian arc and the rest of Alaska were studied in detail by *Nakamura et al.* [1977] and *Nakamura and Uyeda* [1980]. They concluded that the stress regime generally changes from compressional in the thrust zone close to the trench to shear along the volcanic arc landward to tensional in the back arc. They proposed that flank eruptions for polygenetic volcanoes can be regarded as the result of a large-scale natural magma-fracturing experiment [*Nakamura et al.*, 1977] and derived a direction of N60°W ±15° for the maximum compressional horizontal stress near Akutan. This is roughly parallel to the direction of relative motion between the Pacific and North American Plates in the region, and to the orientation of ground cracks that formed during the March 1996 swarm (N70°W). The strike of tension cracks is expected to develop along the maximum compressional stress direction.

We conclude that the March 1996 earthquake swarm was caused primarily by the intrusion of ~0.2 km^3 of magma into a deep reservoir (~13 km) beneath the west flank of Akutan volcano. Sudden pressurization of the reservoir in turn triggered the propagation of a magma-filled dike to within <1 km of the surface and uplifted the western part of the island. The best evidence for intrusion is the pattern of extensional ground cracks that strongly suggests tumescence of the volcano's northwest flank during the swarm. Much less certain is the cause of subsidence elsewhere on the island. One possibility is that magma intrusion beneath the volcano increased extensional strain and/or decreased pore pressure beneath the eastern part of the island.

The strong cluster of earthquakes beneath the head of Akutan Harbor might represent the activation of existing normal faults in response to stresses caused by the intrusion of magma beneath Akutan volcano. Unfortunately, the poor accuracy of earthquake locations from March 18 to July 26, 1996, prevents a more detailed interpretation. Similar clusters of earthquakes have been observed at comparable distances from volcanoes where intrusions were occurring [see, e.g.,

Table 2. Parameters for Best Fitting Model[a]

	One Mogi Source		One Dike Source	Two Sources	
	Deep	Shallow		Mogi	Dike
X coordinate, km	6.47	6.92	4.38	5.94	4.66
Y coordinate, km	10.68	14.08	13.68	8.08	13.78
Depth, km	13.4	2.66	0.008	13.4	0.47
Strike Azimuth, deg	-	-	N63W	-	N73W
Dip, deg	-	-	79.1 NE	-	82.1 NE
Along-strike slip, mm	-	-	0.0 (fixed)	-	0.0 (fixed)
Up-dip slip, mm	-	-	0.0 (fixed)	-	0.0 (fixed)
Expansion, mm	-	-	2517	-	2551
Length, km	-	-	6.21	-	6.66
Width, km	-	-	3.43	-	2.00
Injected Volume, km^3	0.90	0.019	0.054	0.237	0.034
Shift 1 – Shift 2, mm	-67.2	265	302	138	
Variance, mm^2	3036	1306	474	388	
Variance Reduction, %	84.0	93.0	97.6	98.0	
$\Sigma e^2, 10^8$ mm^2	1.30	0.558	0.202	0.166	
Signal Modeled, %	92	96	98.6	99	

[a]Distances (x, y, depth) are measured with respect to the southwest corner of the area shown in Plate 3. Depth of the dike is to the top.

Harlow et al., 1996; *Aspinal et al.*, 1998; *Dvorak and Dzurisin*, 1997]. The earthquakes beneath the eastern part of Akutan Island probably do not indicate the presence of magma but rather movement along existing faults or some other process such as the reduction of pore pressure within the groundwater system, accompanied by subsidence.

Earthquakes that continued to occur beneath Lava Point and the summit caldera from August 1996 to December 1998 may represent continued stress adjustments to the March 1996 intrusion. The apparent shoaling of hypocenters beneath the caldera suggests that this area may be too hot to support brittle failure below a depth of 3-4 km.

Numerical modeling of the 1996 deformation field at Akutan volcano proved to be challenging, in spite of the fact that SAR interferometry provided much more geodetic information than is typically available for such an event. The pattern of seismicity shown in Figures 2 and 3 suggests that multiple deformation episodes contributed to the overall field imaged in Plate 1 and modeled in Plate 3. In the future, a new generation of radar satellites with more frequent passes and better orbit control (yielding shorter baselines and thus more useable image pairs) might make it possible to distinguish among separate deformation events that occur over timescales of a few months, such as those represented in Figures 3a and 3b. However, heavy snow cover during the March 1996 swarm would still preclude separation of the deformation events recorded in Figure 2, which spans just 5 days.

The interferograms presented here provide a rare glimpse of surface deformation associated with intrusive processes beneath an island arc volcano. Often such effects are obscured by subsequent eruptive activity. In this case, even though no eruption occurred, the picture that emerges is complicated and not fully understood. Nonetheless, our results suggest that SAR interferometry has the potential to elucidate not only shallow magma bodies that feed eruptions but also their intrusive underpinnings.

5. Conclusions

Using repeat-pass SAR interferometry, we successfully imaged a complex pattern of ground deformation associated with an earthquake swarm beneath Akutan Island in March 1996. Two interferograms that span the swarm reveal asymmetric uplift of Akutan volcano on the west side of the island and subsidence on the east side. Tumescence of the volcano was caused by inflation of a deep magma reservoir and intrusion of a shallow, steeply dipping dike to within a few hundred meters of the surface beneath the volcano's summit area and northwest flank. Subsidence of the east side of the island may have been caused by extensional strain and/or depressurization of the groundwater system, triggered by inflation or magma movements beneath the west side. This scenario is generally consistent with the deformation pattern revealed by interferograms, the mapped pattern of ground cracks, the distribution of earthquake hypocenters, and the regional stress regime.

No ground movements greater than one interferometric fringe (2.83 cm) were observed outside the caldera in several interferograms for periods of 4 years before or 2 years after the 1996 earthquake swarm. Inside the caldera, localized subsidence by as much as 10 cm during 1992-1993 and 1996-1998 seems to be associated with a zone of active fumaroles. Subsidence is attributed to depressurization or fluid loss from a shallow hydrothermal system beneath the fumaroles.

We conclude that satellite radar interferometry is a useful tool for measuring the deformation of Aleutian volcanoes, at least where lava flows predominate, but only during or between relatively short Alaskan summers. For the technique to become an effective volcano monitoring tool, however, shorter imaging repeat times (of the order of a few days rather than weeks) and longer-wavelength radars (for example, 24-cm L-band like JERS-1 SAR) are essential. Realization of this potential must await the launch of new satellites with missions dedicated at least partly to radar interferometry.

Acknowledgments. ERS-1 and ERS-2 SAR images are copyright © 1992, 1993, 1995, 1996, 1997, and 1998 ESA. SAR data used in this study were supported by the NASA grant NAG5-4369, and provided by the Alaska SAR Facility (ASF). Lu was supported by the USGS contract 1434-CR-97-CN-40274. Wicks, Power, and Dzurisin were supported by the USGS Volcano Hazards Program. We thank the staff at User Services of ASF for their special efforts in making the SAR data available; D-PAF/ESA for providing precision satellite restitute data; P. Delaney, S. Jonsson, and R. Burgmann for careful and constructive reviews; W. Thatcher, T. Albright, C. Werner, and J. Freymueller for useful discussions; F. Amelung for suggestion to invert for the static shift in the range change between patches; D. Gesch, M. Oimoen, and M. Choate for helping us access the Akutan DEM; and D. H. Richter, A. Jolly and P. Stelling for discussions on ground cracks.

References

Alaska Sportsman, From Ketchikan to Barrow, Aug., p.18, 1949.

Aspinal, W.P., A.D. Miller, L.L. Lynch, J.L. Latchman, R.C. Stewart, R.A. White, and J. Power, Soufriere Hills eruption, Montserrat, 1995-1997: Volcanic earthquake locations and fault plane solutions, *Geophys. Res. Lett.*, *25*, 3397-3400, 1998.

Delacourt, C., P Briole, and J. Achache, Tropospheric corrections of the SAR interferograms with strong topography: Application to Etna, *Geophys. Res. Lett.*, *25*, 2849-2852, 1998.

Dvorak, J., and D. Dzurisin, Volcano geodesy: The search for magma reservoirs and the formation of eruptive vents, *Rev. Geophys.*, *35*, 343-384, 1997.

Endo, E.T., S.D. Malone, L.L. Noson, and C.S. Weaver, Locations, magnitudes, and statistics of the March 20 -- May 18 earthquake sequence, in *The 1980 Eruptions of Mount St. Helens, Washington*, edited by P.W. Lipman and D.R. Mullineaus, *U.S. Geol. Surv Prof. Pap*, *1250*, 93-107, 1981.

Feigl, K., and E. Dupre, RNGCHN: A program to calculate displacement components from dislocations in an elastic half-space with applications for modeling geodetic measurements of crustal deformation, *Comput. and Geosci.*, *25*, 695-704, 1999.

Finch, R.H., Akutan volcano, *Z. Vulkanol.*, *XVI*, 155-160, 1935.

Fujiwara, S., P. A. Rosen, M. Tobita, and Mak. Murakami, Crustal deformation measurements using repeat-pass JERS-1 synthetic aperture radar interferometry near the Izu Peninsula, Japan, *J. Geophys. Res.*, *103*, 2411-2426, 1998.

Gesch, D., Topographic data requirement for EOS global change research, *U.S. Geol. Surv. Open File Rep.*, *94-626*, 1994.

Goldstein, R., H. Zebker, and C. Werner, Satellite radar interferometry: Two-dimensional phase unwrapping, *Radio Sci.*, *23*, 713-720, 1988.

Harlow, D. H., J. A. Power, E. P. Laguerta, G. Ambubuyog, R. A. White, and R. P. Hoblitt, Precursory seismicity and forecasting of the June 15, 1991, eruption of Mount Pinatubo, in *Fire and Mud, Eruptions and Lahars of Mount Pinatubo, Philippines*, edited by C. G. Newhall and R. S. Punongbuyan, *285-306*, Univ. of Wash. Press, Seattle, 1996.

Jonsson, S., et al., A shallow-dipping dike fed the 1995 flank eruption at Fernandina volcano, Galapagos, Observed by satellite radar interferometry, *Geophys. Res. Lett.*, *26*, 1077-1080, 1999.

Lanari, R., P. Lundgren, and E. Sansosti, Dynamic deformation of

Etna volcano observed by satellite radar interferometry, *Geophys. Res. Lett.*, *25*, 1541-1544, 1998.

Lu, Z., and J. Freymueller, Synthetic aperture radar interferometry coherence analysis over Katmai volcano group, Alaska, *J. Geophys. Res.*, *103*, 29,887-29,894, 1998.

Lu, Z., D. Mann, and J. Freymueller, Satellite radar interferometry measures deformation at Okmok Volcano, *Eos Trans. AGU*, *79*(39), 461, 467-468, 1998.

Lu, Z., D. Mann, J. Freymueller, and D. Meyer, Synthetic aperture radar interferometry of Okmok volcano, Alaska 1: Radar observations, *J. Geophys. Res.*, *105*, 10,791-10,806, 2000a.

Lu, Z., C. Wicks, D. Dzurisin, W. Thatcher, J. Freymueller, S. McNutt, and D. Mann, Aseismic inflation of Westdahl volcano, Alaska, revealed by satellite radar interferometry, *Geophys. Res. Lett.*, *27*, 1567-1570, 2000b.

Lu, Z., et al., Deformation of New Trident volcano measured by ERS-1 SAR interferometry, Katmai national Park, Alaska, *Geophys. Res. Lett.*, *24*, 695-698, 1997.

Massonnet, D., P. Briole, and A. Arnaud, Deflation of Mount Etna monitored by spaceborne radar interferometry, *Nature*, *375*, 567-570, 1995.

Massonnet, D., and K. Feigl, Radar interferometry and its application to changes in the Earth's surface, *Rev. Geophys.*, *36*, 441-500, 1998.

Massonnet, D. and T. Rabaute, Radar interferometry: Limits and potentials, *IEEE Trans. Geosci. Rem. Sens.*, *31*, 455-464, 1993.

Miller, T.P., R.G. McGimsey, D.H. Richter, J.R. Riehle, C.J. Nye, M.E. Yount, and J.A. Dumoulin, Catalog of the historically active volcanoes of Alaska, *U.S. Geol. Surv. Open File Rep., 98-582*, 1998.

Mogi, K., Relations between the eruptions of various volcanoes and the deformations of the ground surface around them, *Bull. Earthquake Res. Inst. Univ. Tokyo*, *36*, 99-134, 1958.

Nakamura K., and S. Uyeda, Stress gradient in arc-back regions and plate subduction, *J. Geophys. Res.*, *85*, 6419-6428, 1980.

Nakamura, K., K. H. Jacob, and J. N. Davies, Volcanoes as possible indicators of tectonic stress orientation–Aleutians and Alaska, *Pure Appl. Geophys.*, *115*, 87-112, 1977.

Newhall, C. G., and D. Dzurisin, Historical unrest at large calderas of the world, *U.S. Geol. Surv. Bull.*, *1855*, 1108 pp., 1988.

Okada, Y., Surface deformation to shear and tensile fault in an elastic half-space, *Bull. Seismol. Soc. Am.*, *75*, 1135-1154, 1985.

Power, J. A., J. C. Lahr, R. A. Page, B. A. Chouet, and C. D. Stephens, Seismic evolution of the 1989–1990 eruption sequence of Redoubt Volcano, Alaska, *J. Volcanol. Geotherm. Res.*, *62*, 69–94, 1994.

Power, J. A., A. D. Jolly, R. A., Page, and S. R. McNutt, Seismicity and forecasting of the 1992 Eruptions of Crater Peak Vent, Mount Spurr Volcano, Alaska: An overview, in *The 1992 Eruptions of Crater Peak Vent, Mount Spurr Volcano, Alaska*, edited by T.E.C. Keith, *U.S. Geol. Surv. Bull.*, *2139*, 149–159, 1995.

Power, J.A., J.F. Paskievitch, D.H. Richter, and R.G. McGimsey, 1996 seismicity and ground deformation at Akutan volcano, Alaska, *Eos, Trans., AGU*, *77*(46), Fall Meet. Suppl., F514, 1996.

Press, W., S. Teukolsky, W. Vetterling, and B. Flannery, *Numerical Recipes in C: The Art of Scientific Computing*, 994 pp., Cambridge Univ. Press, New York, 1992.

Richter, D.H., C.F. Waythomas, R.G. McGimsey, and P.L. Stelling, Geologic map of Akutan Island, Alaska, *U.S. Geol. Surv. Open File Rep., 98-135*, 22 pp. + 1 plate, 1998.

Rosen, P.A., S. Hensley, H.A. Zebker, F.H. Webb, and E.J. Fielding, Surface deformation and coherence measurements of Kilauea Volcano, Hawaii, from SIR-C radar interferometry, *J. Geophys. Res.*, *101*, 23,109-23,125, 1996.

Sigmundsson, F., H. Vadon, and D. Massonnet, Readjustment of the Krafla spreading segment to crustal rifting measured by satellite radar interferometry, *Geophys. Res. Lett.*, *24*, 1843-1846, 1997.

Sigmundsson, F., P. Durand, and D. Massonnet, Opening of an eruptive fissure and seaward displacement at Piton de la Fournaise volcano measured by RADARSAT satellite radar interferometry, *Geophys. Res. Lett.*, *26*, 533-536, 1999.

Thatcher, W., and D. Massonnet, Crustal deformation at Long Valley Caldera, eastern California, 1992-1996, inferred from satellite radar interferometry, *Geophys. Res. Letts.*, *24*, 2519-2522, 1997.

Vadon, H., and F. Sigmundsson, Crustal deformation from 1992 to 1995 at the Mid-Atlantic Ridge, southwest Iceland, mapped by satellite radar interferometry, *Science*, *275*, 193-197, 1997.

Wicks, C., W. Thatcher, and D. Dzurisin, Migration of fluids beneath Yellowstone Caldera inferred from satellite radar interferometry, *Science*, *282*, 458-462, 1998.

Zebker, H., P. Rosen, and S. Hensley, Atmospheric effects in interferometric synthetic aperture radar surface deformation and topographic maps, *J. Geophys. Res.*, *102*, 7547-7563, 1997.

D. Dzurisin, U.S. Geological Survey, David A. Johnston Cascades Volcano Observatory, 5400 MacArthur Blvd., Vancouver, WA 98661. (dzurisin@usgs.gov)

Z. Lu, Raytheon STX Corporation, U.S. Geological Survey, EROS Data Center, Sioux Falls, SD 57198. (lu@usgs.gov)

J. Power, U.S. Geological Survey, Alaska Volcano Observatory, 4200 University drive; Anchorage, AK 99508. (jpower@usgs.gov)

C. Wicks Jr., U.S. Geological Survey, 345 Middlefield Rd. MS 977, Menlo Park, CA 94025-3591. (cwicks@usgs.gov)

(Received November 10, 1999; revised May 7, 2000; accepted June 1, 2000.)